CHINESE OPTICS LETTERS

Vol. 22, No. 4 | April 2024

Picosecond gain-switched polymer fiber random lasers

Wenyu Du (杜文彧)[1], Sen Gao (高 森)[2], Xiaojuan Zhang (张小娟)[1], Siqi Li (李思祺)[1], Yan Kuai (蒯 雁)[1], Zhiqiang Wang (王治强)[1], Zhigang Cao (曹志刚)[1], Feng Xu (徐 峰)[1], Yu Liu (刘 宇)[1], Lin Xu (徐 林)[1], Junxi Zhang (张俊喜)[2], Kang Xie (谢 康)[3], Benli Yu (俞本立)[1], and Zhijia Hu (胡志家)[1*]

[1] Information Materials and Intelligent Sensing Laboratory of Anhui Province, Key Laboratory of Opto-Electronic Information Acquisition and Manipulation of Ministry of Education, School of Physics and Opto-electronics Engineering, Anhui University, Hefei 230601, China

[2] School of Instrument Science and Opto-electronics Engineering, Laboratory of Optical Fibers and Micro-nano Photonics, Hefei University of Technology, Hefei 230009, China

[3] School of Opto-electronic Engineering, Zaozhuang University, Zaozhuang 277160, China

*Corresponding author: zhijiahu@ahu.edu.cn

Received November 16, 2023 | Accepted January 6, 2024 | Posted Online April 17, 2024

Random lasers are a type of lasers that lack typical resonator structures, offering benefits such as easy integration, low cost, and low spatial coherence. These features make them popular for speckle-free imaging and random number generation. However, due to their high threshold and phase instability, the production of picosecond random lasers has still been a challenge. In this work, we have developed three dyes incorporating polymer optical fibers doped with various scattering nanoparticles to produce short-pulsed random fiber lasers. Notably, stable picosecond random laser emission lasting 600 ps is observed at a low pump energy of 50 μJ, indicating the gain-switching mechanism. Population inversion and gain undergo an abrupt surge as the intensity of the continuously pumped light nears the threshold level. When the intensity of the continuously pumped light reaches a specific value, the number of inversion populations in the "scattering cavity" surpasses the threshold rapidly. Simulation results based on a model that considers power-dependent gain saturation confirmed the above phenomenon. This research helps expand the understanding of the dynamics behind random medium-stimulated emission in random lasers and opens up possibilities for mode locking in these systems.

Keywords: random laser; polymer optical fiber; gain-switched laser; picosecond pulse.
DOI: 10.3788/COL202422.040603

1. Introduction

Random lasers (RLs) are lasers that can be generated without conventional resonators. The light amplification of RLs is realized by multiple scattering feedback, for example, in laser crystals or amorphous powders[1,2]. Due to their low cost, compact size, and simple integration, RLs have received extensive research attention[3,4]. Among many RL systems, polymer fiber RLs possess unique advantages. Two-dimensional confinement from fiber waveguide geometry significantly enhances multiple scattering through total internal reflection, resulting in RLs with a lower threshold, directionality, and integrated simplicity. Furthermore, polymers effortlessly combine various gain materials and scattering structures by doping materials to control RLs. Researchers are highly interested in RLs based on polymer optical fibers (POFs) for these two reasons. Hu's team first reported POF-based RLs in 2013[5], followed by demonstrations of polarized RLs using oriented POFs in 2016[6]. In addition, the team also demonstrated real-time temperature-controlled RLs based on POFs[7]. The stability and tunability of the RLs based on POF were demonstrated through these investigations, indicating their vast potential for use in sensors, optical switches, and speckle-free imaging.

Most RL research has focused on their frequency-domain characteristics. However, studying RLs in the time domain is also crucial, particularly for their dynamics[8–11]. In 2002, Cao's team investigated the dynamic response of RLs and discovered that the emission pulse width narrows significantly when pump energy surpasses the lasing threshold[12]. Several subsequent works have explored short pulse generation and the time-domain characteristics of RLs. For instance, in a glass cuvette filled with a dye solution, the Alfano group achieved a 50 ps pulse width using a 230 μJ pumping[13]. Pecoraro *et al.* analyzed the time-emission characteristics of rhodamine-doped hybrid powder using photomultiplier tubes and found that the generation of RLs results in a narrower time distribution[14]. Shi *et al.* observed two inflection points in the temporal profile associated with the operating threshold and laser mode conversion as pump energy increased. They also observed a coherent RL's pulse width of 5.03 ns in vertically pumped random silver

nanowire–dye solution lasers at a pump energy of 97.13 mW/cm^2[15,16].

Conventional lasers usually use gain-switching or *Q*-switching mechanisms to generate high repetition rate pulse sequences in the nanosecond or picosecond range[17–19]. *Q*-switched laser generation usually requires electro-optic crystals, acousto-optic devices, or saturable absorption materials. Gain-switching is advantageous because it does not require additional intracavity components, making it suitable for compact system designs[20]. Moura *et al.*[21] demonstrated the replication of the symmetry-breaking phenomenon and spontaneous mode locking in multimode *Q*-switched Nd:YAG lasers with scatters instead of resonant cavities. But there are no random media and the phase is different from the glassy state of the incoherent oscillation mode of an RL. Self-initiated mode locking was first achieved experimentally by Antenucci *et al.*, who discovered the presence of nonlinear mode-locked coupling in RLs[22]. This nonlinear mode-locked coupling was observed in spatially overlapping resonances that are highly dependent on frequency-matching conditions. While these works contribute to understanding the dynamics of RL emission, picosecond RLs based on gain-switching mechanisms have not been reported.

In this work, we generated picosecond and low-threshold POF RLs based on the gain-switching mechanism. First, three POFs doped with different scattering nano-particles (NPs) were prepared using the Teflon mold. Then, we employed the gain-switching mechanism to obtain stable RL pulse outputs in the picosecond range. Notably, the pulse widths of RLs are an order of magnitude narrower than that of pumped nanosecond pulses. Furthermore, we observed that the emission characteristics in the time domain were influenced by the polarization angle of the RLs, facilitating the study of amplified spontaneous emission (ASE) and RL emission dynamics. To our knowledge, this is the first analysis of the time- and frequency-domain properties of polymer fiber-based RLs and the first report of gain-switched picosecond RLs. Additionally, the pulse width of 0.6 ns is one of the shortest reported RL pulse widths. Our study introduces an innovative approach by introducing the gain-switching mechanism to picosecond RLs based on POFs, which has not been previously reported for RLs.

2. Results and Discussion

The gain medium and the scattering system are the key elements to constitute RLs. We doped the gain medium (the laser dye PM597), and the scattering nanoparticles into the core of POF to fabricate POF-based RLs. To evaluate the stability and reliability of the short-pulse RL, three different scattering systems were designed, wherein three distinct types of scattering particles were doped in the POF, namely, polyhedral oligomeric silsesquioxanes (POSS) NPs, Fe_3O_4@SiO_2 core-shell NPs, and Au NPs. The cladding material for all disordered POFs consists of a copolymer of methyl methacrylate (MMA) and butyl acrylate (BA) at an 80:20 volume ratio, while the core material is MMA and BA at a volume ratio of 85:15 with a laser dye mass fraction of 0.14%. The core dopant mass fractions of POSS NPs, Fe_3O_4@SiO_2 NPs, and Au NPs are 22.9%, 2.0%, and 0.05%, respectively. Optical micrographs of the end face of POSS NPs-doped POF (POPOF), Fe_3O_4@SiO_2 NPs-doped POF (FePOF), and Au NPs-doped POF (AuPOF) are shown in Figs. 1(a)–1(c). The details of the corresponding POFs are listed in Table 1.

The measurement setup is illustrated in Fig. 1(d). A *Q*-switched Nd:YAG laser (532 nm, pulse duration 6 ns, repetition rate 10 Hz, spot diameter 100 μm) serves as the pump source, and a Glan prism group is used to regulate the pump energy intensity. The pump light is coupled spatially to a 3 cm-long POF through a focusing lens. The pump energies in the experiments are all below the damage threshold of the POFs. The mixture of pump light and RL light is then emitted from the other end surface. A filter with a cut-off wavelength of 550 nm filters out the excess pump light. Subsequently, a mirror directs the RL light to a beam splitter (50:50) through another focusing lens. An optical fiber probe couples 50% of the RL light to a microspectrometer (QE65PRO, Ocean Optics, resolution ~0.4 nm, integration time 100 ms) for measuring the spectra. The angle of the pump light entering the fiber and the angle to receive RL are identical for the three POFs in the experiment. The remaining 50% of the RL light is received by the silicon

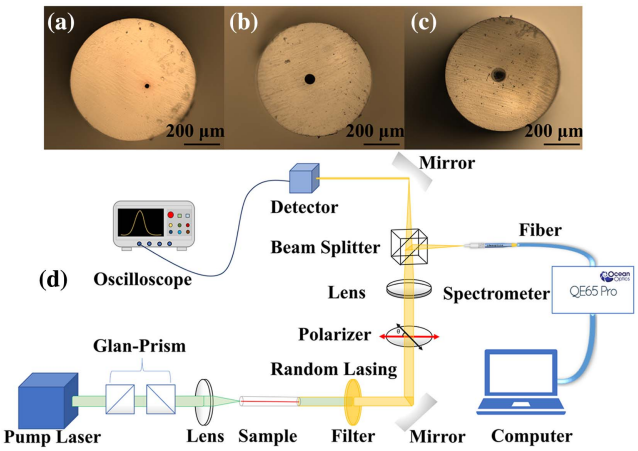

Fig. 1. Optical micrographs of three types of disordered POF cross sections, corresponding to (a) POPOF, (b) FePOF, and (c) AuPOF; (d) experimental setup for testing RL emission.

Table 1. Parameters of POFs.

	Size of Doped NPs (nm)	Core Size (μm)	Cladding Size (μm)
POPOF	200	26.7	696.4
FePOF	10 nm Fe_3O_4@5 nm SiO_2	59.5	637.2
AuPOF	29	68.4	639.5

photodetector with a bandwidth of 2 GHz and a rise time of 150 ps (Thorlabs DET025A/M). The voltage signal is then transmitted to an oscilloscope (RIGOL DS6104) with a bandwidth of 1 GHz to collect the RL signal in the time domain. The pulse width measured in the experiment is within the detection range of the photodetector and oscilloscope. This setup can simultaneously detect the signal of RLs in the frequency and time domains, thereby considerably minimizing measurement error.

Figure 2 presents the RL emission spectra of POPOF, FePOF, and AuPOF at different pump energies in Figs. 2(a), 2(c), and 2(e), respectively. Additionally, Figs. 2(b), 2(d), and 2(f) show the integral intensities of Figs. 2(a), 2(c), and 2(e) at different pump energies, respectively. Because the phenomenon for the three kinds of POFs is similar, here we provide a detailed analysis of POPOF. Figure 2(a) shows broad fluorescence emission at low pump energy, which evolves into a narrow gain peak at the central wavelength of 568.2 nm when the pump energy exceeds the threshold. Furthermore, multiple sharp lasing peaks appear at the top of the emission peak, as customary for coherent RLs, to represent various laser modes originating from several closed-scattering loop cavities[23]. Figure 2(b) depicts the integrated emission intensities as a function of the pump energy for the polymer fiber RL system, where the nonlinear dependence of the emission intensity on the pump energy indicates lasing action. A noticeable inflection point is observed in Fig. 2(b), corresponding to the threshold of about 40.79 μJ. The threshold

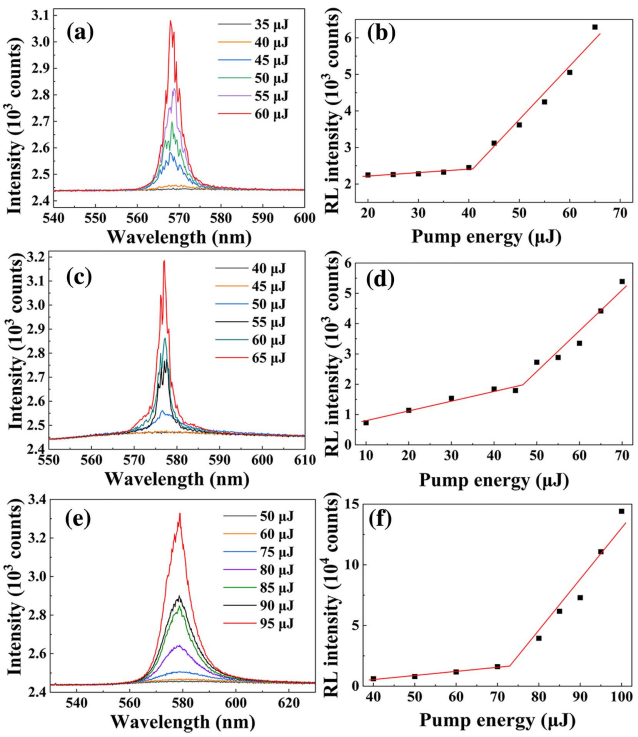

Fig. 2. RL emission property of three POFs. The emission spectrum variations with pump energy of POPOF, FePOF, and AuPOF are shown in (a), (c), and (e), respectively. The variations of integral intensity with pump energy of POPOF, FePOF, and AuPOF are shown in (b), (d), and (f), respectively.

for FePOF and AuPOF is approximately 46.72 μJ and 72.95 μJ, respectively. The three types of random fiber lasers vary regarding the number of laser modes, the emission wavelength of the peaks, and the threshold value. The RL spectrum based on POPOF exhibits more peaks and the lowest threshold, since the doping concentration of POSS NPs is the highest, resulting in the smallest scattering mean free path and facilitating the generation of the RL. FePOF-based RL spectra contain fewer spikes and slightly higher thresholds than POPOF. Figures 2(a) and 2(b) demonstrate several modes in the random lasing spectrum, indicating the production of typical coherent RLs. AuPOF-based RLs, with the lowest doping concentration, demonstrate a non-coherent RL with fewer peaks on the top of its spectrum. It has the highest threshold compared with the other two RLs. This implies that the RL based on AuPOF does not form closed scattering loop cavities to form coherent RLs. Moreover, the picosecond RLs exhibit a lower threshold compared to conventional lasers due to their lack of a traditional resonator structure. The scattering cavity of the RL necessitates less energy for pumping than multiple reflections in traditional resonators. Furthermore, the disordered scattering is significantly amplified through total internal reflection owing to the two-dimensional confinement of the polymer waveguide geometry, reducing the threshold.

Figures 3(a), 3(c), and 3(e) are the normalized time distributions of POPOF, FePOF, and AuPOF, respectively, reflecting the process of RLs from the establishment to decay in the time domain. The pulse widths under different pump energy are shown in the second column. The time distribution curve fluctuates due to the rapid photodetector's typical response[23]. The normalized time distribution was fitted with a Gaussian function, and Fig. 3(b) illustrates the link between the pump energy of the POPOF-based RL and the time distribution pulse width. The red dotted line represents the corresponding threshold in Fig. 2(b). The time signal starts to grow quickly when the pump light's energy reaches 23 μJ. When the energy increases, the pulse width decreases from 6.4 ns at 23 μJ to 2.4 ns at 38 μJ, which is narrower than the pump pulse width of 6 ns. This phenomenon indicates that short-pulse RLs are beginning to build. The primary mode of PM597 emission dynamics is stimulated emission when the pump energy is significantly higher than the threshold. At pump energy of 50 μJ, the pulse width decreases to 0.6 ns, demonstrating the entire establishment of the short-pulse RLs. At pump energy of 50–65 μJ, the pulse width of the time pulse tends to be stabilized. Table 2 illustrates the variation of pulse width and decay time with pump energy for the three types of RLs. As the pump energy increases from below to above the threshold, the decay time and pulse width reduce by an order of magnitude. Specifically, the fall time of POPOF-based RL decreases from 19.9 ns at 23 μJ to 2.3 ns at 50 μJ. At sufficiently high pump energy, the pulse widths of all three types of POFs can be less than 1 ns. Although these three RLs have varying peaks and thresholds and produce distinct types of RLs owing to different scattering structures, they all eventually generate picosecond RL pulses, as evidenced by Figs. 2 and 3.

Upon excitation by a pump laser pulse, the laser dye molecules undergo a transition from the ground state to the excited

Table 2. Single Exponential Decay Fitting of Temporal Properties.

POF	Pump Energy (μJ)	Fall Time (ns)	Pulse Width (ns)
POPOF	23	19.9	6.4
	38	11.6	2.4
	50	2.3	0.6
FePOF	37	20.4	5.8
	40	8.6	1.5
	45	2.1	0.7
AuPOF	65	18.4	6.6
	80	12.8	2.4
	90	3.4	0.7

state. This results in an exponential growth of populations at the upper energy level and a rapid increase in fluorescence form in the time domain followed by a gradual decline. The competition between RL gain and loss is dependent on gain saturation, which is influenced by the pump pulse energy; higher pump energy yields more gain than loss, and vice versa. The gain medium is stimulated until population inversion reaches the threshold; at this point, the gain switch is activated, allowing a large amount of optical energy to flow through the gain medium. Consequently, there is a sudden increase in population inversion and gain. When the continuous pump light intensity approaches the threshold level, the pump pulse light superimposed on laser dye molecules causes the number of reversing particles in the "scattering cavity" to rapidly exceed the threshold. This leads to an increase in excited radiation output, generating a picosecond random laser pulse. The rate equation is used to describe the time-dependent gain g,

$$\frac{\mathrm{d}g}{\mathrm{d}t} = \frac{g_0 - g}{\tau_g} - \frac{g|\psi(t)|^2}{E_g}, \tag{1}$$

where τ_g is the lifetime of the gain medium. Since τ_g is much longer than the pulse duration, the energy transferred to the pulse cannot be replenished immediately, resulting in gain loss during the generation of the pulse. g_0 is the small signal gain and E_g is the gain saturation energy. $\psi(t)$ is the pulse envelope. The pulse width of the pump laser is 6 ns, while the pulse width of RL is only about 0.6 ns. Since τ_g of the gain medium is much longer than the pulse duration time, the energy transferred to the RL pulse cannot be replenished in time, and the gain is depleted during the pulse passing through the gain medium in the fiber core. The red line indicates this process in Fig. 4(a). The blue line is the pump pulse and the green line is the fluorescent pulse before the pump energy exceeds the threshold of random lasing. $\psi_F(t)$ is the pulse envelope of the fluorescence emission. The gain of the laser dye is time-varied as the pump pulse passes through the fiber. During the formation of the fluorescent pulse, the gain at the tail of the pulse is less than that at the front as the red line in Fig. 4(a). Therefore, this effect can change the envelope of the pulse, causing the fluorescent pulse to move forward compared to the pump pulse as the green curve shows, but it does not change the phase velocity[24]. After the pulse energy is further increased above the threshold, the pulse width of the RL becomes narrower. The pulse envelope of the RL pulse $\psi_R(t)$ can be expressed as

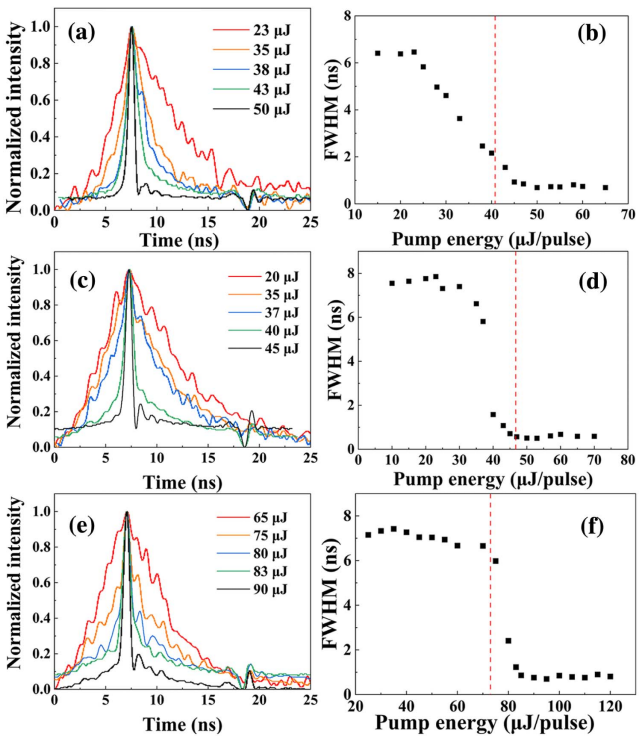

Fig. 3. RL pulse characteristic of polymer fibers. The normalized time distributions for POPOF, FePOF, and AuPOF are shown in (a), (c), and (e), respectively. The emission pulse widths of POPOF, FePOF, and AuPOF are shown in (b), (d), and (f), respectively. The red dotted line represents the threshold for the random lasing emission spectrum.

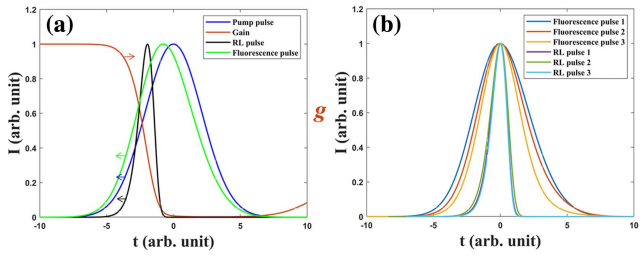

Fig. 4. (a) Simulation of gain and RL pulse compression. The red line is the gain curve of the RLs. The blue line is the pump laser pulse. The green line is the fluorescence pulse below the threshold. The black line is the RL pulse. (b) Simulation of pulse width variation when pump energy is below and above the threshold.

$$\psi_R(t) = \psi(t) \cdot \exp\left(\frac{g}{2} z\right). \tag{2}$$

The ordinary differential Eq. (1) is solved using the Runge–Kutta method[25]. When the pump energy increases, the value E_g is modified accordingly in our model, and the narrowing of the pulse can be observed, as shown in Fig. 4(b). The existing simulation model, which accounts for a slow power-dependent gain-switching mechanism, does not consider the impact of disordered scattering on RL pulse width. As a result, the experimental result narrowing degree is smaller than the simulated pulse width.

We analyzed the normalized intensity distribution of picosecond pulses of RLs based on POFs. Figure 5(a) demonstrates that the repetition rate of the RL based on POFs is identical to that of the pump laser, which is 10 Hz, indicating gain-switched pulsed laser characteristics. We utilized the dual channels of the oscilloscope to capture the pulses of both random and pump lasers, as illustrated in Fig. 5(b). The delay time of the random laser pulses compared to the pump laser pulses is 2 ns when the pump energy is 50 μJ, implying rapid activation of the gain switch in the POF-based RL. In conventional lasers, short pulses are generated via gain switching by modulating the pump power. *Q*-switching modulates cavity losses to achieve short pulses, which initially involve low levels of fluorescence and require amplification in a round trip of multiple resonators before transmitting pulses with a certain time delay. RLs lack the traditional resonant cavity structure, and their emission is governed by random multiple scattering in the photon gain medium. This means that feedback and light amplification rely solely on the gain medium and disordered scattering medium. Consequently, the build-up time in the scattering cavity is much shorter than the oscillation time in the conventional resonant cavity, allowing for the rapid build-up of short RL pulses with no delay relative to the pump pulse. The picosecond RL pulse is rapidly established within 2 ns after the pump laser pulse is generated. In traditional lasers, the delay time of the laser pulse relative to the pump pulse exceeds 100 ns[26].

In Fig. 6(a), we pumped POPOF, FePOF, and AuPOF with energies of 50, 45, and 90 μJ, respectively. It was observed that the pulse widths of all the RLs based on POF remained stable between 0.6 and 0.8 ns after 35,000 consecutive pumping pulses.

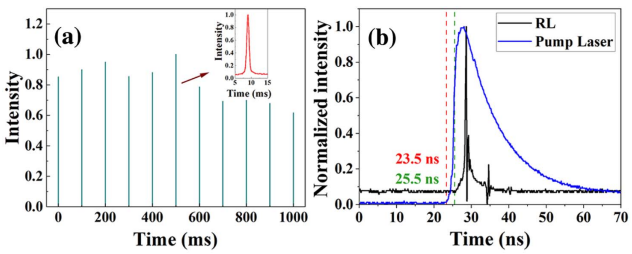

Fig. 5. (a) Normalized periodic distribution of short pulse RLs within 1 s. Inset, an enlarged view of an RL pulse. (b) Simultaneous acquisition of pump laser and RL pulses.

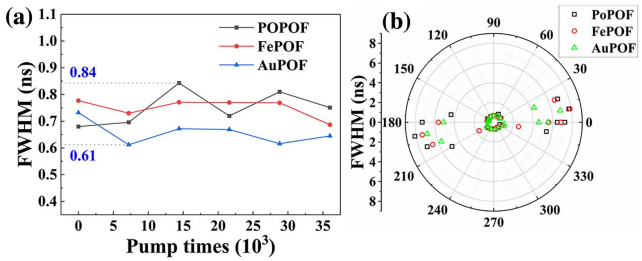

Fig. 6. (a) Linewidth of the three POFs at 35,000 pumps; (b) the pulse width of RLs varies with the angle θ.

This indicates the stability of the picosecond RLs over a long period of pumping time. The small fluctuations in pulse width were caused by 4% fluctuations in the pump laser energy. In Fig. 6(b), we investigated the relationship between the polarization direction of RLs and their pulse width. We positioned a polarizer in front of the photodetector and aligned it with the polarization direction of the pump laser. We define the rotation angle of the polarizer at this time to be 0°. By changing the angle θ of the polarizer, we observed that the partially polarized RLs had the most significant duration spread at polarization angles of 10° and 190°, corresponding to the lowest intensity of the RLs. When the polarization angle θ was between 60° and 150° or between 240° and 330°, short pulses lasting less than 1 ns were obtained. These results indicate that the strongest vibration direction of the POF-based picosecond RL is at an angle to the pump light. The emitted light combines RL and ASE light, with RL dominating at pulse widths less than 1 ns and ASE dominating at wider pulse widths.

3. Conclusion

In conclusion, gain-switched RLs with a pulse width of 0.6 ns are generated using specially designed POFs. The lowest threshold is reached at a minimum of 40.79 μJ. The effectiveness and reliability of the gain-switching mechanism in POF-based RLs are demonstrated via three different scattering regimes. Stable short-pulse RL emission is observed, demonstrating consistency with the pump pulse frequency. The effect of polarization angle on RL duration is also investigated, proving that the emitted light is a mixture of RL and ASE light. Gain-saturation model simulations confirm the narrowing phenomenon of the RL pulse relative to the pump pulse, shedding insight into the gain-switching dynamics of polymer fiber-based RL. This work obtains one of the shortest pulses of RL and offers a new perspective on short-pulse RL generation and its emission dynamics.

Acknowledgements

This work was supported by the National Natural Science Foundation of China (Nos. 12174002, 11874012, 11874126, and 51771186), the Excellent Scientific Research and Innovation Team of Anhui Province (No. 2022AH010003), the Key

Research and Development Plan of Anhui Province (No. 202104a05020059), the Innovation Project for the Returned Overseas Scholars of Anhui Province (No. 2021LCX011), the University Synergy Innovation Program of Anhui Province (No. GXXT-2020-052), and the Anhui Young Wanjiang Scholars Talent Project (No. Z010118167).

References

1. S. Garcia-Revilla, J. Fernandez, M. Barredo-Zuriarrain, *et al.*, "Diffusive random laser modes under a spatiotemporal scope," Opt. Express **23**, 1456 (2015).
2. W. Gao, T. Wang, J. Xu, *et al.*, "Robust and flexible random lasers using perovskite quantum dots coated nickel foam for speckle-free laser imaging," Small **17**, 2103065 (2021).
3. T. Zhai, X. Zhang, Z. Pang, *et al.*, "Random laser based on waveguided plasmonic gain channels," Nano Lett. **11**, 4295 (2011).
4. Z. Hu, H. Zheng, L. Wang, *et al.*, "Random fiber laser of POSS solution-filled hollow optical fiber by end pumping," Opt. Commun. **285**, 3967 (2012).
5. Z. Hu, B. Miao, T. Wang, *et al.*, "Disordered microstructure polymer optical fiber for stabilized coherent random fiber laser," Opt. Lett. **38**, 4644 (2013).
6. Z. Hu, Y. Liang, X. Qian, *et al.*, "Polarized random laser emission from an oriented disorder polymer optical fiber," Opt. Lett. **41**, 2584 (2016).
7. Z. Hu, J. Xia, Y. Liang, *et al.*, "Tunable random polymer fiber laser," Opt. Express **25**, 18421 (2017).
8. M. Asuncion Illarramendi, J. Zubia, I. Bikandi, *et al.*, "Pump-polarization effects in dye-doped polymer optical fibers," J. Light. Technol. **36**, 4090 (2018).
9. S. Garcia-Revilla, I. Sola, R. Balda, *et al.*, "Two-photon pumped random lasing in a dye-doped silica gel powder," Proc. SPIE **7598**, 759804 (2010).
10. S. John and G. Pang, "Theory of lasing in a multiple-scattering medium," Phys. Rev. A **54**, 3642 (1996).
11. X. Jiang and C. M. Soukoulis, "Time dependent theory for random lasers," Phys. Rev. Lett. **85**, 70 (2000).
12. C. M. Soukoulis, X. Jiang, J. Y. Xu, *et al.*, "Dynamic response and relaxation oscillations in random lasers," Phys. Rev. B **71**, 041103 (2005).
13. W. L. Sha, C. H. Liu, and R. R. Alfano, "Spectral and temporal measurements of laser action of Rhodamine 640 dye in strongly scattering media," Opt. Lett. **19**, 1922 (1994).
14. E. Pecoraro, S. Garcia-Revilla, R. A. S. Ferreira, *et al.*, "Real time random laser properties of Rhodamine-doped di-ureasil hybrids," Opt. Express **18**, 7470 (2010).
15. X. Shi, Q. Chang, J. Tong, *et al.*, "Temporal profiles for measuring threshold of random lasers pumped by ns pulses," Sci. Rep. **7**, 5325 (2017).
16. Z. Wang, X. Shi, S. Wei, *et al.*, "Two-threshold silver nanowire-based random laser with different dye concentrations," Laser Phys. Lett. **11**, 095002 (2014).
17. J. Tian, G. Weng, and Y. Liu, "Gain-switching in $CsPbBr_3$ microwire lasers," Commun. Phys. **5**, 160 (2022).
18. R. I. Woodward, Y. S. Lo, and M. Pittaluga, "Gigahertz measurement-device-independent quantum key distribution using directly modulated lasers," npj Quantum Inf. **7**, 58 (2021).
19. M. Jiang and P. Tayebati, "Stable 10 ns, kilowatt peak-power pulse generation from a gain-switched Tm-doped fiber laser," Opt. Lett. **32**, 1797 (2007).
20. J. Yang, Y. Tang, and J. Xu, "Development and applications of gain-switched fiber lasers," Photonics Res. **1**, 52 (2013).
21. A. L. Moura, P. I. R. Pincheira, and A. S. Reyna, "Replica symmetry breaking in the photonic ferromagneticlike spontaneous mode-locking phase of a multimode Nd:YAG laser," Phys. Rev. Lett. **119**, 163902 (2017).
22. F. Antenucci, G. Lerario, and B. S. Fernandez, "Demonstration of self-starting nonlinear mode locking in random lasers," Phys. Rev. Lett. **126**, 173901 (2021).
23. H. Zhang, H. Zhang, C. Yang, *et al.*, "Ultra-photo-stable coherent random laser based on liquid waveguide gain channels doped with boehmite nanosheets," Photonics Nanostruct. **28**, 75 (2018).
24. T. Xian, W. Wang, and L. Zhan, "Real time revealing relaxation dynamics of ultrafast mode-locked lasers," Phys. Rev. Res. **4**, 013202 (2022).
25. F. X. Kurtner, J. A. Au, and U. Keller, "Mode-locking with slow and fast saturable absorbers-what's the difference?" IEEE J. Sel. Top. Quantum Electron. **4**, 159 (1998).
26. M. Jiang and T. Parviz, "Stable 10 ns, kilowatt peak-power pulse generation from a gain-switched Tm-doped fiber laser," Opt. Lett. **32**, 1797 (2007).